International Journal of Applied Earth Observations and Geoinformation 112 (2022) 102879

Contents lists available at ScienceDirect

International Journal of Applied Earth Observations and Geoinformation

journal homepage: www.elsevier.com/locate/jag

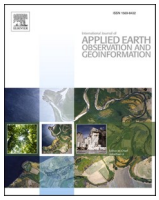

Application of the two-source energy balance model with microwave-derived soil moisture in a semi-arid agricultural region

Yanhao Xu [a,b], Lisheng Song [a,b,*], William P. Kustas [c], Kejia Xue [b], Shaomin Liu [d], Mingguo Ma [b], Tongren Xu [d], Long Zhao [b]

[a] Key Laboratory of Earth Surface Processes and Regional Response in the Yangtze-Huaihe River Basin, Anhui Province, School of Geography and Tourism, Anhui Normal University, 241002, China
[b] Chongqing Jinfo Mountain Karst Ecosystem National Observation and Research Station, School of Geographical Sciences, Southwest University, Chongqing 400715, China
[c] USDA, Agricultural Research Service, Beltsville Agricultural Research Center, Hydrology and Remote Sensing Lab, 10300 Baltimore, Ave. BARC-West, Bldg. 007, Beltsville, MD 21738, USA
[d] State Key Laboratory of Earth Surface Processes and Resource Ecology, Faculty of Geographical Sciences, Beijing Normal University, Beijing 100875, China

ARTICLE INFO

Keywords:
TSEB-SM
TSEB
Soil moisture stress
Validation
Intercomparison

ABSTRACT

Evapotranspiration (*ET*) is a critical component of the water, carbon and energy cycles of the land surface. Remote sensing-based models provide the possibility of mapping *ET* from field to regional and even global scales. A key boundary condition of the Two-Source Energy Balance (TSEB) model for computing *ET* is land surface temperature (LST). The proposed modification to TSEB is to use a combination of near surface soil moisture (SM) derived by microwave and LST as dual boundary conditions along with a more physically-based transpiration formulation for computing *ET*. Both TSEB and TSEB-SM were applied to an irrigated agricultural area with surrounding semi-arid sparse natural vegetation. In general, TSEB-SM model performance when compared to measured fluxes was similar to the TSEB model. However, the TSEB-SM model computed more reliable estimates of *LE* under dry soil surface/low vegetation cover conditions, primarily in the arid and semiarid natural ecosystems surrounding the irrigated agricultural area. These comparisons indicate that TSEB-SM may provide more reliable flux estimation and *ET* partitioning over sparsely vegetated areas compared to the traditional formulations used in TSEB. With reliable microwave remote sensing of soil moisture, TSEB-SM has potential for *ET* monitoring in both natural and agricultural landscapes.

1. Introduction

Land surface evapotranspiration (*ET*) includes transpiration by plants and evaporation of intercepted water contributed by plant surfaces, water surfaces, and from the soil. It is an integral part in the Earth's energy system linking the water and carbon cycles (Oki and Kanae 2006; Rigden and Salvucci 2017). In fact, most of the precipitation will return to the atmosphere in the form of *ET*, which accounts for 2/3 of the global annual average precipitation and *ET* accounts for nearly 60% of the available energy on the land surface (Bastiaanssen et al., 2007; Trenberth et al., 2009).

Arid and semi-arid regions occupy about 40% of the global terrestrial surface, and they contain nearly 40% of the world's population (Reynolds et al., 2007). A distinguishing feature of these regions is that they are strongly affected by the periodic droughts, which often results in water and food shortages, and environmental degradation (Fensholt et al., 2012). Therefore, monitoring evapotranspiration in arid with semi-arid regions leading to improvements in water use efficiency can lead to better water resource management in agricultural regions (Kustas and Anderson 2009).

The methods to estimate *ET* include ground observations primarily by eddy covariance (EC), remote sensing (RS)-based methods, and land surface models (Liu et al., 2016). Among them, remote sensing-based approaches have shown the greatest potential in mapping spatially-distributed *ET* from field to regional, even global scales (Feng et al., 2020). In the light of this, numerous remote sensing-based *ET* models of

* Corresponding author at: Key Laboratory of Earth Surface Processes and Regional Response in the Yangtze-Huaihe River Basin, Anhui Province, School of Geography and Tourism, Anhui Normal University, 241002, China.
E-mail addresses: songls@ahnu.edu.cn, songls@swu.edu.cn (L. Song).

https://doi.org/10.1016/j.jag.2022.102879
Received 19 September 2021; Received in revised form 12 June 2022; Accepted 19 June 2022
Available online 30 June 2022

varying complexity that have been proposed. One of the more widely applied and tested models over various land covers and climates is the Two-Source Energy Balance (TSEB) model which is mainly attributed to the model being physical-based but with key inputs readily available from current remote sensing data (Guzinski et al. 2020). Nevertheless, it has been reported that the TSEB can overestimate *ET* in arid and semi-arid areas often containing sparse natural vegetation and in some cases underestimate *ET* over irrigated agriculture in semi-arid regions where the physiological and advection processes will directly affect the rate of transpiration and/or efficiency of sensible heat transport (Gonzalez-Dugo et al., 2009; Li et al., 2018b; Song et al., 2016). About 65% of land evapotranspiration is contributed by plant-mediated transpiration via leaf stomatal conductance (Liu et al., 2020), which is specifically affected by hydroclimatic stress influenced by available soil water content and the atmospheric vapor pressure deficit (VPD) (Green et al., 2019; Xu et al., 2021). Therefore, beyond the important boundary conditions of land surface temperature (LST) and leaf area index (LAI), incorporating soil moisture information and a more physically-based transpiration formulation is proposed in this study to improve the soil evaporation estimate and better constrain the plant transpiration in the TSEB model. This is expected to also improve partitioning of *ET* into its component of evaporation and transpiration.

The main objectives of this paper are: (i) Coupling soil moisture information from airborne microwave observations and incorporating a new transpiration algorithm into the original TSEB model (TSEB-SM) over a semi-arid agricultural area. (ii) Comparing the performance of TSEB and TSEB-SM from field to landscape scale using observations from a large aperture scintillometer (LAS) providing a source area encompassing several kilometers and EC flux tower measurements reflecting *ET* over various landcover types.

2. Methodology

2.1. Tseb

Norman et al (1995) proposed the original version of TSEB model, which has been followed by a number of refinements to improve its utility over a wide range of complex surfaces. In the TSEB scheme, the total surface energy budget equation can be separately expressed for the soil surface and plant canopy:

$$Rns = Hs + LEs + G0 \tag{1}$$

$$Rnc = Hc + LEc \tag{2}$$

In addition, combined with the method proposed by Kustas and Norman (1999), Rn_s and Rn_c can be calculated as:

$$Rnc = (1 - \tau longwave)(L\downarrow + \varepsilon s\sigma T_s^4 - 2\varepsilon_c\sigma T_c^4) + (1 - \tau solar)(1 - \alpha c)S\downarrow \tag{3}$$

$$Rns = \tau longwavL\downarrow + (1 - \tau longwave)\varepsilon c\sigma T_c^4 - \varepsilon s\sigma T_s^4 + \tau solar(1 - \alpha s)S\downarrow \tag{4}$$

where the Rn_s, Rn_c, H_s, H_c, LE_s, LE_c are the net radiation, sensible heat flux, latent heat flux from soil and canopy, respectively. G_0 is the mean the soil heat flux. $\tau_{longwave}$ and the τ_{solar} are the longwave and shortwave radiation transmittances through the canopy. $L_\downarrow$ and $S_\downarrow$ are the incoming longwave and shortwave radiation from the sky. In this study, the downwelling longwave radiation was calculated using the air temperature (Campbell and Norman, 1998). ε_s and ε_c are the emissivity of soil and canopy, σ is the Stefan-Boltzman constant, always equal to 5.67×10^{-8} W·m^{-2}·K^{-4}. The values of α_s, α_c are the albedos for canopy and soil, calculated according to the ratios of diffuse and direct radiation over their surfaces (Campbell and Norman, 1998). *T* is the temperature which the subscript *c* and *s* represent the canopy and soil, respectively.

The initial canopy and soil temperatures are partitioned from LST using estimated fraction of soil and canopy and combined with the Priestly-Taylor equation applied to the canopy as an initial estimate of the canopy transpiration, with coefficient a_c value equal to 1.26 (Eqs. (5) and (6)). The vegetation and soil sensible heat fluxes can be determined by estimating the aerodynamic resistance of the soil and canopy, and by determining the temperature and net radiation of the soil and canopy (Eqs. (8),9 and 10). Then, the energy balance of the canopy system is computed and LE_s is solved as a residual (Eqs. (11) and (12)) with G_0 taken as a fraction of Rn_s. Notably, the a_c value is adjusted to decline gradually if the canopy is stressed and not transpiring at the potential rate estimated using the Priestly-Taylor equation with $a_c \sim 1.26$, causing the non-physical solution of LE_s less than 0 which indicates condensation on the soil surface during daytime conditions. The a_c value is incrementally reduced until a solution is reached where $LE_s \geq 0$.

$$Tci = Ta + \frac{RncRa}{\rho Cp}\left[1 - acfg\frac{\Delta}{\Delta + \gamma}\right] \tag{5}$$

$$LST^4\varepsilon = fc\varepsilon CT_c^4 + [1 - fc]\varepsilon ST_s^4 \tag{6}$$

In the above equations, T_{ci} is the initial temperature of the canopy, T_a is the air temperature, R_a is the aerodynamic resistance to heat transport from the canopy space to the reference air temperature, ρ means the air density, C_p is the air heat capacity, f_g is the fraction of green vegetation, Δ is the slope of the temperature curve and saturation vapor pressure, and γ is the psychrometric constant equaling approximately 0.06. LST is the input data obtained from MODIS, ε is the emissivity can be obtained by combining vegetation emissivity (ε_c) and soil emissivity (ε_s) through the equation (7) and *fc* is fraction of vegetation coverage calculated from LAI (Anderson et al. 2005).

$$\varepsilon = \varepsilon cf_c + (1 - f_c)\varepsilon s \tag{7}$$

The equations for computing H_s and H_c including their sum *H,* are as follows:

$$Hs = \rho CP\frac{Ts - Tac}{Rs} \tag{8}$$

$$Hc = \rho CP\frac{Tc - Tac}{Rx} \tag{9}$$

$H = HC + HS$(10) In the above equations, the value of T_{ac} is the temperature in the canopy air space, R_s is the aerodynamic resistance of soil, while R_x represents the canopy aerodynamic resistance.

In the TSEB model, the soil heat flux, G_0, is presumed to be a ratio of the soil net radiation, the ratio value equaling approximately 0.3 around noon time (Kustas et al., 1998). Thus, given the Rn_s, Rn_c, H_s, H_c and G_0, the soil evaporation and canopy transpiration are derived from the soil and vegetation surface energy balance (Norman et al., 1995).

$$LES = RnS - HS - G0 \tag{11}$$

$$LEC = RnC - HC \tag{12}$$

2.2. TSEB-SM

Using the Priestley-Taylor parameterization for estimating canopy transpiration does not always guarantee a reliable solution, and so having additional model constraints such as surface soil moisture observations to estimate soil evaporation and a more physically based transpiration algorithm may improve the estimates of *ET* and *E*, *T* partitioning (Kustas et al., 2003b). Following this reasoning, two key modifications to TSEB were proposed: a more physically-based stomatal conductance parameterization, and a soil wetness factor to better estimate *ET* partitioning into canopy transpiration (*T*) and soil evaporation (*E*) under a wide range of soil moisture content conditions. Song et al. (2016) proposed a soil wetness factor ($f_{s\text{-}song}$) for partitioning soil temperature under advective conditions and is expressed as follows:

$$fs-song=\frac{2}{1+(\frac{\theta}{\theta 0})^{-2}} \tag{13}$$

where the θ is the near surface volumetric water content which is derived from passive microwave remote sensing (~5 cm depth), and the θ_0 is the water content at field capacity.

A similar analytical soil wetness factor ($f_{s\text{-}merlin}$) was proposed by (Merlin et al., 2011), and can be expressed as follows:

$$fs-merlin=\frac{1}{2}-\frac{1}{2}\cos(\frac{\theta}{\theta\max}\pi) \tag{14}$$

with θ_{max} defined as the saturated water content. Both $f_{s\text{-}song}$ and $f_{s\text{-}merlin}$ represent a water stress factor (boundary condition) on soil evaporation, which may improve the performance of TSEB by incorporating an additional constraint on soil evaporation. However, these two moisture stress factors use different boundary conditions to explain the water stress. It was proposed to combine the two algorithms to define a soil moisture stress factor (f_s). This is similar to the soil water stress scheme in the GLEAM (Global Land Evaporation Amsterdam Model) (Martens et al. 2017) to compensate for the limitation of $f_{s\text{-}song}$ and $f_{s\text{-}merlin}$ (Song et al.,2022). Details for defining f_s can be found in (Song et al.,2022) and f_s can be calculated as follows.

$$fs=\sqrt{fs-song\times fs-merlin} \tag{15}$$

Stomatal conductance plays a significant role in plant transpiration. To characterize the limitation of soil water to the plant transpiration, the canopy stomatal conductance stress factor ($\frac{gstress}{ga}$) was defined and can be calculated as follows, refer to De Kauwe et al. (2014) and Leuning (1995):

$$\frac{gstress}{ga}=\frac{g0\times LAI+1.6(1+\frac{g1\times fs}{\sqrt{VPD}})\ \frac{A}{Cs}}{g0\times LAI+1.6(1+\frac{g1}{\sqrt{VPD}})\ \frac{A}{Cs}} \tag{16}$$

where $g_0=0.01molH_2Om^{-2}s^{-1}$, is the default stomatal conductance when photosynthesis equals 0 (De Kauwe et al., 2014). The stomatal stress factor can be scaled to the canopy by accounting for LAI, and using the plant functional type dependent conductance g_1 which are the same values as those defined in GABLE (Community Atmosphere Biosphere Land Exchange) (Kowalczyk et al., 2006; De Kauwe et al., 2014). g_a is the leaf aerodynamic conductance under non-water stress conditions. C_s is CO_2 concentration on the leaf surface and was estimated from an average of observations from the eddy covariance tower network at the time of the satellite overpass, *VPD* is vapor pressure deficit, and *A* is leaf photosynthetic rate which can be calculated according to BEPS (Boreal Ecosystem Productivity Simulator) model (Chen et al., 1999). The values of T_c and T_s can be expressed as follows in TSEB-SM scheme:

$$Tc=Ta+\frac{RncRa}{\rho cp}(1-\mathrm{ac}fg\frac{gstress}{ga}\frac{\Delta}{\Delta+\gamma}) \tag{17}$$

$$Ts=Ta+\frac{(Rns-G0)(Ra+Rs)}{\rho cp}(1-asfs\frac{\Delta}{\Delta+\gamma}) \tag{18}$$

where a_s is the Priestley-Taylor coefficient of soil with a value of 1.0 (Agam et al., 2010; Tanner and Jury 1976). Then, the estimated T_c and T_s are combined using Eq (6) to compute a land surface temperature, and the difference between aggregated temperature and observed land surface temperature were added to the estimated T_c and T_s values, respectively, in order to force agreement between modeled and observed LST in the TSEB-SM model. Given the derived T_c and T_s, the rest of the calculation processes of surface heat fluxes, including Rn_c, Rn_s, H_c, H_s, LE_c, LE_s, and G_0, are same to the calculation in the TSEB model.

3. Study area and data acquisition

3.1. Characteristics of the study area

The study area located in the midstream of Heihe river watershed which is the second-largest (143,000 km^2) continental river in the northwestern China and contains a wide variety of land covers. In the middle of the basin lies a desert-oasis zone with a predominantly irrigated agricultural area surrounded by the desert landscape. This desert-oasis zone contains a full range of soil moisture content and is therefore an ideal experiment area to evaluate the TSEB-SM model. The whole region has a temperate continental climate, in the middle of the basin, the annual mean air temperature ranges from approximately 6 ℃ to 8 ℃ (Li et al. 2018a), the annual precipitation is between 100 mm and 250 mm (Cheng et al., 2013) but the potential evaporation can be from 1,200 mm to 1,800 mm (Huang et al., 2015). In 2012, a Multi-Scale Observation Experiment on Evapotranspiration (MUSOEXE) was conducted as part of the HiWATER (Heihe Water Allied Telemetry Experimental Research) project (HiWATER-MUSOEXE) over a period from May 3 to September 21 in this desert-oasis zone (Liu et al., 2016). The flux observation network comprised of 21 flux towers (Fig. 2). All except site 21 (wetland), are used to evaluate the performances of TSEB and TSEB-SM models.

3.2. Model inputs and study method

Model input data included satellite data comprised of 1 km LST acquired by MODIS (Moderate-resolution Imaging Spectroradiometer) the version of MOD11A1 product (https://modis.gsfc.nasa.gov/), and LAI derived from GLASS (Global Land Surface Satellite) products (http://www.glass.umd.edu/), with spatial resolution of 1 km. The meteorological data including atmospheric pressure, air temperature, wind speed, relative humidity and solar radiation were derived by interpolating the measurements from the network of AWS stations co-located with the EC stations. Vegetation height was estimated from ground data collected during HiWATER-MUSOEXE experiment. In this study, two days of observations, DOY182 and DOY192, were selected as input data. These two days had microwave observations with good weather conditions, namely clear skies, warm temperatures, and light winds. For DOY 182, air temperature was approximately 27 ℃, the wind speed was light at about 2–3 m/s, and the shortwave radiation was about 700 W/m^2 during the flight. For DOY 192, the air temperature was about 26 ℃, with lighter winds of around 1 m/s and the radiation was similarly around 700 w/m^2 during the flight. For the surface soil moisture data required by TSEB-SM model, airborne measurements from the Polarimetric L-band Multibeam Radiometer (PLMR) sensor with a resolution of 1 km were used (Li et al., 2015). For a detailed description of soil moisture retrieval from the PLMR sensor, the reader is referred to Li et al. (2015). The surface energy balance data, including *Rn*, *H*, *LE*, G_0 from EC flux tower measurements, the G_0 are derived by converting the measured soil heat flux to surface and *H* measured from the four pairs of LAS systems can be downloaded from the web site https://data.tpdc.ac.cn/zh-hans/ (Liu et al., 2011).

In this study, the TSEB and TSEB-SM models are applied using the same input data, while the TSEB-SM required additional information on the surface soil moisture and CO2 concentration. Model output from TSEB and TSEB-SM are compared and evaluated with measurements from EC flux towers. However, since the spatial resolution of model output is1 km (see below) there is a spatial scale mismatch with EC flux tower observations which have a contributing source area typically within a few hundred meters. Therefore, the model output of sensible heat flux was also compared to LAS observations which have a source area that can cover several kilometers. A detailed flow chart describing of model inputs, output and validation is illustrated in Fig. 1.

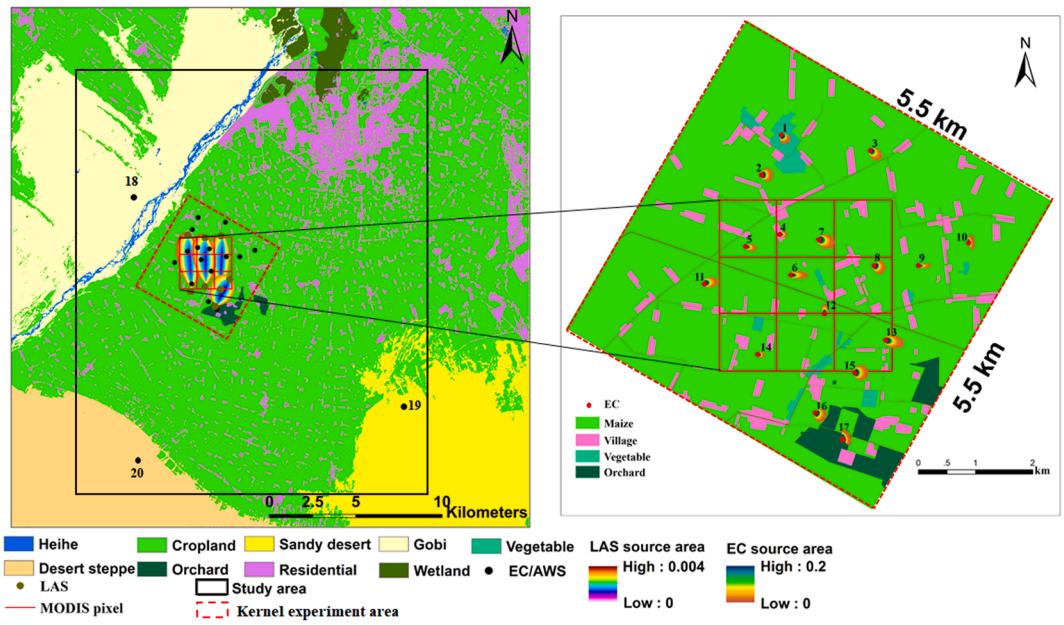

Fig. 1. Land cover map of the HiWATER-MUSOEXE study area, locations of the EC towers/ automatic weather stations and LAS systems including footprint of EC stations.

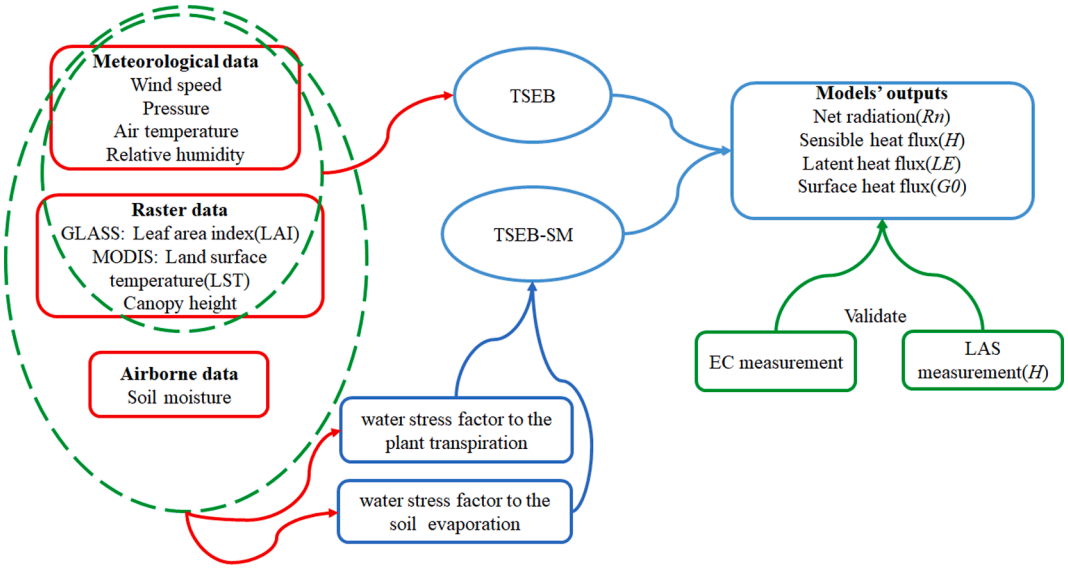

Fig. 2. The flowchart that illustrating schemes of TSEB and TSEB-SM validated with surface flux observation.

4. Results

4.1. Comparison with EC system measurements

The eddy covariance technique is widely used to measure *ET* over homogeneous surfaces. According to the surface energy conservation principle, the sum of the turbulent fluxes, namely sensible and latent heat fluxes (*H* and *LE*) measured from the EC should be equal to the surface available energy ($Rn\text{-}G_0$). But on account of local or non-local factors affecting turbulent transport, neglecting additional terms to the surface energy balance and sensor design issues, it typically results in ($H + LE$) < ($Rn\text{-}G_0$) (Foken 2008). Here, the Bowen ratio method (Twine et al., 2000) which assumes both *H* and *LE* are undermeasured but the relative partitioning of the available energy ($Rn\text{-}G_0$) is assumed reliable and was used to force energy balance closure. These adjusted *H* and *LE* were used to evaluate the model performance.

The scatterplot shown in Fig. 3 illustrates the comparison of modeled surface fluxes from TSEB and TSEB-SM with EC measurements along with near surface (~5 cm) soil water content conditions estimated from the passive microwave at satellite overpass times. TSEB-SM tends to have better agreement with EC measured surface heat fluxes, particularly under lower surface soil moisture conditions (Fig. 3). At the sites 18, 19, 20 which are the points denoted by the red circles in Fig. 3, the ground observation values of *LE* corrected by the Bowen ratio energy closure are 131, 145 and 150 W/m^2, respectively, with an average of 142 W/m^2. The TSEB model output for sites 18, 19 and 20 are 335, 321, and 259 W/m^2, respectively, with an average of 305 W/m^2. In contrast, output of TSEB-SM model is 185, 162, and 115 W/m^2, respectively with the average value of 154 W/m^2. Furthermore, the TSEB-SM has slightly lower mean absolute percent difference (MAPD) values compared to the TSEB model (Table 1). However, this is mainly caused by a few outliers (cf. Fig. 3) with sparse vegetation cover under lower surface soil

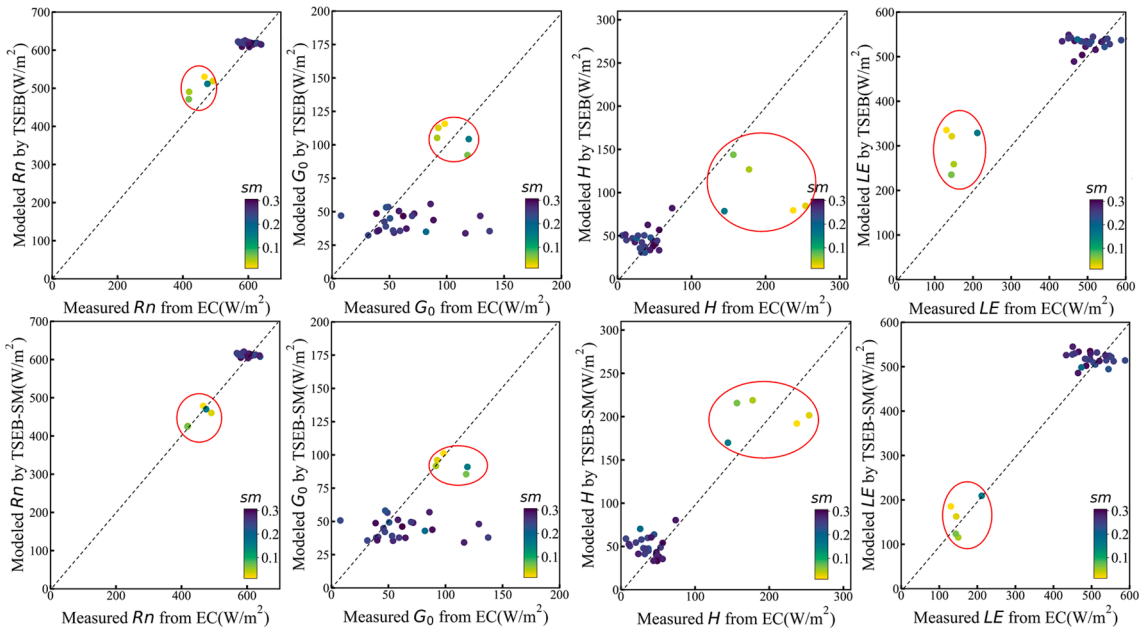

Fig. 3. Scatterplots for comparison of measured net radiation (*Rn*), sensible heat flux (*H*), soil heat flux (G_0), and latent heat flux (*LE*) from the EC systems and estimates from TSEB and TSEB-SM models at satellite overpass times. The points encompassed by the red circles are the arid and semi-arid sparsely vegetated sites 18,19, 20 on DOY 182, and sites 18 and 20 on 192 (site 19 on DOY 192 had no measurements). (For interpretation of the references to colour in this figure legend, the reader is referred to the web version of this article.)

Table 1
Statistical results of the modeled vs. measured surface fluxes.

		Rn (W/m^2)	*H* (W/m^2)	*LE* (W/m^2)	G_0 (W/m^2)
Measured	Mean	576	62	444	70
	SD	58	64	134	31
TSEB	Mean	599	55	492	53
	SD	43	26	90	25
	MBE	−23	7	−47	17
	MAPD	5%	44%	13%	35%
	RMSE	32	49	75	35
TSEB-SM	Mean	586	75	458	52
	SD	61	57	135	19
	MBE	−9	−13	−14	17
	MAPD	3%	40%	8%	33%
	RMSE	22	30	44	34

a Mean is the average value of each flux components, SD is the standard deviation, can be showed with equation.

moisture conditions. Otherwise both TSEB and TSEB-SM model output correspond well with the EC measurements which are mainly under non-water stress conditions (i.e., soil moisture content > 0.25 m^3/m^3). Additionally, most of the EC sites have vegetation fractional cover > 0.7, so the surface soil moisture has minor impact on the surface fluxes.

The divergence between the two models increases under drier conditions with sparse vegetation cover. These are sites 18, 19, 20 are mainly from the sandy desert and Gobi area with dry soil (soil water content typically below 0.1 m^3/m3) and with the fractional vegetation cover estimated by remote sensing to be less than 0.3 with sites 18 and 19 having a peak LAI ~ 0.3 while site 20 had a peak LAI ~ 0.2. The TSEB model underestimates *H* measured by the EC towers yielding in overestimation of *LE*. These extremely low values of LAI indicates that the main source of *LE* is coming from soil evaporation, and consequently the soil aerodynamic resistance significantly affects the computation of *H* and as a result the *LE* estimates. Li et al (2019) found that the default soil aerodynamic resistance formulation for TSEB requires adjusting the coefficients for soil roughness to achieve good agreement in *H* and *LE* and that a new formulation that requires no modification for soil roughness should be applied under these conditions. However, it appears that incorporating soil moisture in the TSEB-SM model appears to compensate for errors caused by using the default soil aerodynamic resistance yielding similar results to the modifications proposed by Li et al (2019) for these sparse canopy cover conditions (Fig. 3).

$SD = \sqrt{\frac{\sum_{x=1}^{n}(x-x1)^2}{n}}$, x is the value of each flux, x_1 is the average value of each flux. MBE is the mean bias error of modeled values and observed values, the compute formula is$MBE = \frac{\sum_{y=1}^{n}(y-y1)}{n}$,$y$ is modeled fluxes, y_1 is measured fluxes. MAPD is the mean absolute percentage difference, can be expressed with$MAPE = \frac{1}{n}\sum_{y=1}^{n}\left|\frac{y-y1}{y}\right|$*100%. RMSE is the root mean square error, the compute formula is$RMSE = \sqrt{\frac{\sum_{y=1}^{n}|y-y1|^2}{n}}$.

4.2. Comparison with LAS measurements

The source area of EC system *H* and *LE* measurements typically encompass a few hundred of meters. In most cases, the land use change and field size are at 100 m scale so that model output at 1 km will contain a mixture of land covers or vegetation cover and soil moisture conditions and not be representative of only the tower footprint. Moreover, the areal extent and location of the flux footprint is affected by many factors including wind direction/wind speed, atmospheric stability, and other turbulence characteristics (Kustas et al., 2001).

For a more consistent comparison of modeled and measured *H* at spatial resolutions commensurate with pixel and model grid size, LAS measurements were used to assess the performance of TSEB and TSEB-SM. The larger flux footprint/source area associated with LAS measurement offers a chance to integrate several modeled *H* pixels representative of the LAS integrated value. In Fig. 4, comparison of *H* estimated from TSEB and TSEB-SM with observations obtained by LAS at the satellite overpass times is illustrated. The output of *H* from TSEB-SM compared to TSEB yield similar difference statistics with both models generally underestimating *H*. Since the LAS measurements mostly comprise the well-irrigated cropland where the soil moisture content and vegetation cover are high, this results in relatively low *H* values ranging from 30 W/m^2 to 60 W/m^2.

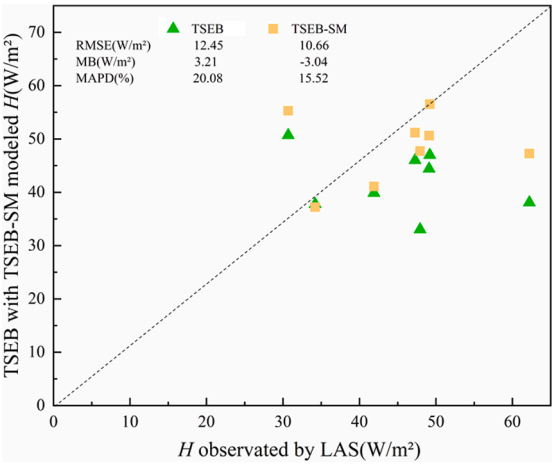

Fig. 4. Comparison of *H* estimates from TSEB (green triangles) and RSEB-SM (brown squares) and the observations by the LAS systems. The LAS source-area encompasses several *H* pixels from TSEB and TSEB-SM that are averaged at satellite overpass times. (For interpretation of the references to colour in this figure legend, the reader is referred to the web version of this article.)

4.3. Comparison of spatial distribution between TSEB and TSEB-SM

Both EC and LAS observations are not able to provide model validation under full range of land cover and soil water content conditions. In order to obtain some insight to surface conditions where there exist significant discrepancies in TSEB and TSEB-SM model output a comparison of flux output on a pixel-by-pixel basis was conducted similar to Choi et al (2009). Maps of *H* and LE along with LAI and surface soil moisture maps are illustrated in Fig. 5.

DOY 182 and DOY 192 were selected with different atmospheric conditions, soil moisture, and vegetation growth stages. The kernel experimental area is within an irrigation district covered by the dense and well-irrigated crops with LAI values ranging from 1.5 to 2.5, and soil water content values greater than 0.15 m^3/m^3 and reaching field capacity at 0.4 m^3/m^3. As a result, very similar spatial distributions of *H* and *LE* are created by the models in the irrigation area. These models compute values of *H* ranging from 20 to 120 W/m^2 and 350 to 650 W/m^2 for *LE*. But surrounding this experimental area is sparse vegetation cover with the LAI value significantly less than 1.0, and surface soil water content values mostly less than 0.15 m^3/m^3. For these areas the two models compute *H* ranging from 70 to 270 W/m^2, while 100 to 400 W/m^2 for *LE*.

In Fig. 5, TSEB-SM tends to have a higher *H* and a lower *LE* values than the TSEB model which is consistent with the results evaluated with EC tower measurements. In Fig. 6 the comparison for pixel-by-pixel of *LE* values estimated by TSEB and TSEB-SM on DOY 182 and DOY 192 are shown. The figures indicate discrepancies in modeled *LE* increases as the soil moisture content decreases, which generally correlates with decreasing vegetation cover and reaches a maximum of approximately 100 W/m2, mainly from the sparsely vegetated semiarid area (Fig. 6).

The largest discrepancies between the two models are under dry surface soil moisture with sparse vegetation cover conditions, where both the differences in latent heat flux of canopy and latent heat flux of soil yield a positive bias, namely TSEB LE_c and especially LE_s > than TSEB-SM output (see Fig. 7). The difference in LE_c and LE_s calculated from TSEB and TSEB-SM illustrated in Fig. 7 are shown as scatter plots in Fig. 8. Overall, the differences in LE_c are larger than the differences in LE_s, and can reach about −190 ~ 180 W/m^2 in the densely vegetated areas. While values of LE_c modeled from TSEB are mostly higher than TSEB-SM, especially in the irrigation area having dense vegetation cover (LAI > 2.5), they tend to be similar outside the irrigation area with lower LAI. However, for the LE_s, values from TSEB-SM are higher than TSEB by about 50 to 100 W/m^2 in the irrigation area, while over the sparse vegetation cover surfaces, the values of LE_s from TSEB-SM are 50 to ~ 170 W/m^2 lower than TSEB (see Fig. 7). Similar results also can be found in Fig. 8, where the values of LE_c and LE_s are similar for higher soil water content at near surface (0–5 cm) values (sm > 0.3 m^3/m^3), especially for the modeled LE_c which correspond to more dense vegetation cover. However, for drier surface (sm less than 0.1 m^3/m^3), the difference in LE_c and LE_s between the two models is more significant. Under this condition, the LE_c modeled by TSEB tends to be greater than TSEB-SM from 50 to100 W/m^2. The LE_s values produced by the two models yield more scatter (Fig. 8). Under wetter near-surface soil moisture (sm ~ 0.2–0.3 m^3/m^3), the TSEB-SM yielded higher values than the TSEB model, averaging around + 50 W/m^2. At dry near-surface low soil moisture conditions (sm < 0.1 m^3/m^3), LE_s values modeled by TSEB-SM are 50 to 100 W/m^2 less than TSEB model. These results suggest that the TSEB-SM modeling version using a physically-based transpiration algorithm and incorporating a soil moisture boundary condition may produce more reliable estimates of not only in *LE* but also in its components of LE_c and LE_s particularly under dry sparsely vegetated conditions.

5. Discussion

In this study, both flux observations and model inter-comparisons suggest that the TSEB-SM can produce more reliable *LE* and *H* estimates than the TSEB model under sparse vegetation cover/dry soil surface conditions. These results are consistent with the former studies

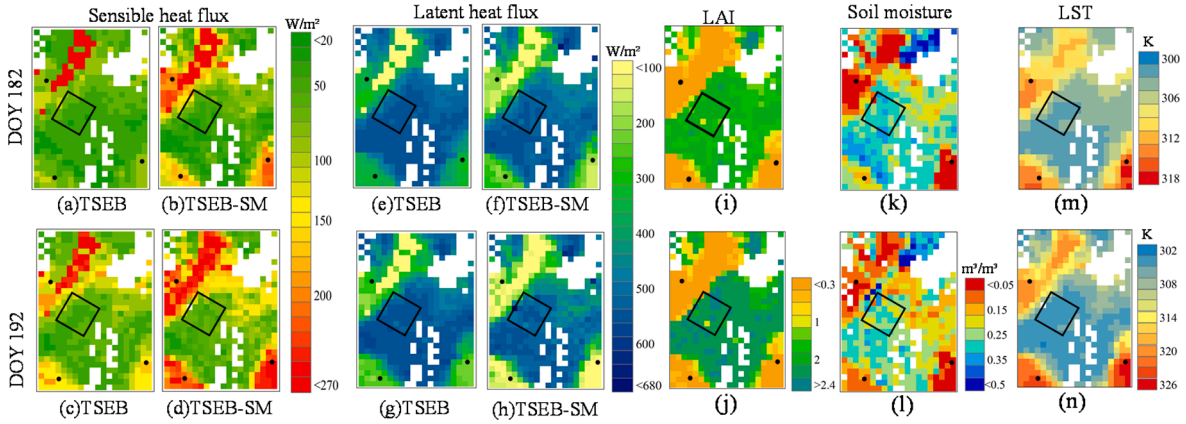

Fig. 5. The spatial pattern of modeled *H* and *LE* from TSEB and TSEB-SM along with LAI and soil moisture maps on DOY 182 and DOY 192. The white areas denote no model output, and the black box is the kernel experimental area with the black solid circles defining the locations of sites 18–20. The areas where LAI exceeds ~ 1 contain irrigated crops.

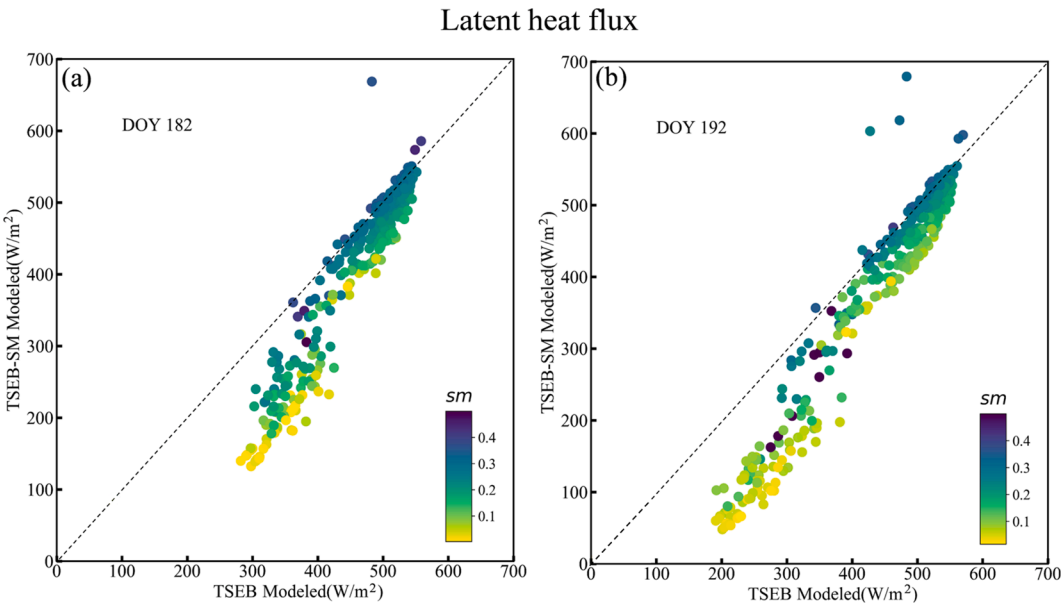

Fig. 6. Comparison of *LE* estimates between TSEB and TSEB-SM for DOY 182 and DOY 192.

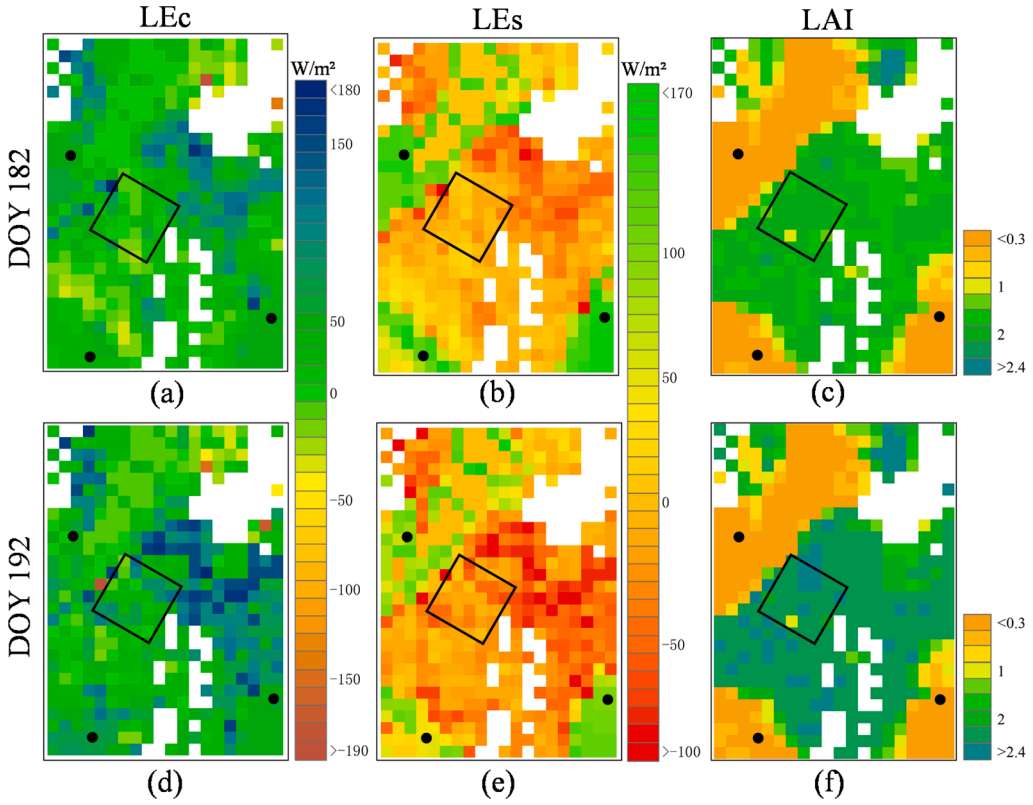

Fig. 7. The spatial distribution of differences in model output (TSEB - TSEB-SM), on DOY 182 and 192 (a), (d) for LE_c, and (b), (e) for LE_s, respectively. The black box is the kernel experimental area, and the black solid circles define the locations of sites 18–20.

in which the soil surface latent heat flux is solved directly by using the surface soil moisture data derived from microwave observations (Ait Hssaine et al., 2018; Kustas et al., 2003a; Li et al., 2006). The TSEB-SM may also produce more reliable partitioned fluxes of transpiration and evaporation under drier surface conditions covered by sparse vegetation cover due to the model explicitly coupling the soil moisture with the LST thus better constraining the water and energy exchange from the soil surface. For the TSEB model it has been shown that the default soil aerodynamic resistance algorithm may not be applicable to sparsely vegetated arid ecosystems (Kustas et al., 2016).

The TSEB-SM model yielded *H* and *LE* consistent with the TSEB model, particularly under the dense vegetation cover/ moist surface soil water content conditions, which can partly solve the overestimation issue in the former studies that only used soil moisture at near surface as critical boundary condition (Li et al., 2006; Ait Hssaine et al., 2021). The TSEB-SM model uses both surface radiometric temperature and near

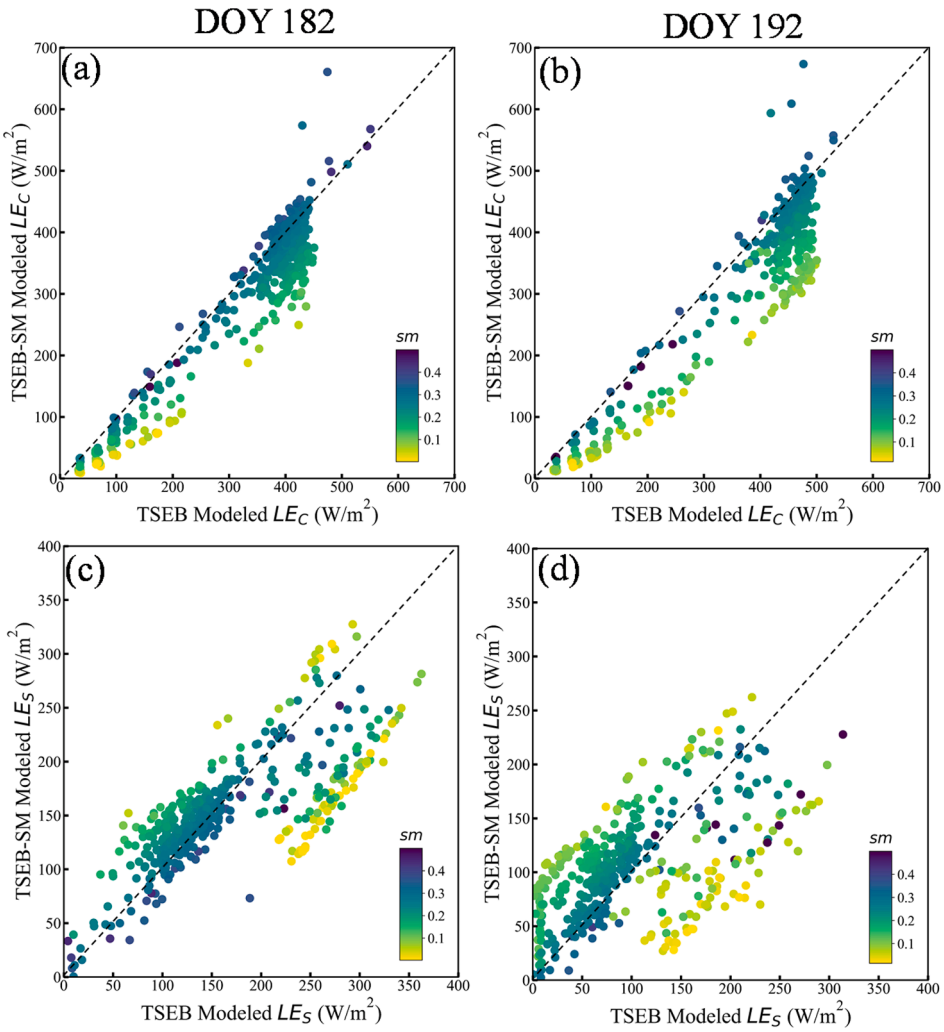

Fig. 8. Comparison of LE_c and LE_s estimates between TSEB and TSEB-SM for DOY 182 and DOY 192.

surface soil water content as boundary conditions, along with a more robust transpiration algorithm to constrain fluxes that come from the soil and canopy, respectively. Consequently, the TSEB-SM model takes advantage of both the thermal and near-surface soil moisture constraints to achieve a solution. This may allow the TSEB-SM model to generate more reliable fluxes over a wider range of soil water content and canopy cover conditions.

In TSEB-SM scheme, the soil temperature was calculated using the Priestley-Taylor equation with the Priestley-Taylor coefficient adjusted by the surface soil moisture information, while the canopy temperature was computed applying the same Priestley-Taylor equation for the canopy similar to TSEB but with the with the Priestley-Taylor coefficient constrained by a canopy stomatal conductance stress factor which can be regulated by the available soil water content. Compared with TSEB, the proposed formulation in TSEB-SM avoids the uncertainty of the Priestley-Taylor coefficient in the generation of vegetation and soil temperatures (Ait Hssaine et al., 2020). On the other hand, a revised soil aerodynamic resistance formulation applied to TSEB over these same desert sites (site 18, 19 and 20) using ground-based LST data was also was shown to dramatically improve the performance of TSEB (Li et al.,2019). Consequently, more investigations are needed in both combining the soil moisture algorithm in TSEB and implementing the revised soil aerodynamic resistance formulations to evaluate overall improvement in TSEB performance.

The better performance of the soil moisture constrained TSEB-SM model over the sparse vegetation cover/dry soil surface conditions may be due in part to the greater accuracy of airborne based PLMR soil moisture retrieval algorithm in areas with lower vegetation density (Entekhabi et al., 2010). The L-band derived PLMR soil moisture data is most sensitive to the surface soil water content under sparse vegetation conditions. But in the irrigated cropland area with LAI values>2.5, the PLMR measurements are likely to have less soil water content sensitivity. The optimal sensitivity of PLMR observations in sparse and dense vegetation coverage, respectively, can partly explain variable performance in *ET* estimation from TSEB-SM model in and outside the irrigated agricultural area (Figs. 5 and 7). In this study, the TSEB-SM model was evaluated with limited number of airborne soil moisture observations. A greater number of PLMR-derived soil moisture observations are needed to better assess TSEB-SM in the higher density vegetation cover conditions.

The spatial resolution of soil moisture and soil moisture depth are two important factors restricting the model application at regional scale. In this study, the soil moisture is derived from airborne observations and the surface heat fluxes only estimated in the irrigation district. Ait Hssaine et al. (2020, 2021) proposed a self-calibrated TSEB-SM method using disaggregated SMOS and MODIS data as inputs. It also can partly resolve the issue of TSEB model which could underestimate the *H* and overestimate *LE* under moderate to dense vegetation cover conditions. The high-resolution soil moisture data disaggregated from coarse microwave-based satellite observations may have better accuracy under the lower vegetation density. However, disaggregated soil moisture products could have gaps in densely vegetated areas due to interference

of the microwave signal by the relatively high vegetation water content. In the future, there is potential for soil moisture products with higher spatial resolution, which were downscaled from coarse satellite data using the MODIS LST (Zhou et al., 2017), LAI products and other factors influencing the distribution and metric of soil moisture (Zhao et al., 2021).

Additionally, the depth of soil moisture is also an important factor affecting the model performance. Soil moisture in the root-zone has a stronger effect on vegetation transpiration, but obtaining soil moisture in the root-zone is very difficult, because it is affected by vegetation rooting characteristics and depth, soil texture variations both horizontally and vertically and uncertainty in inputs from rainfall and irrigation (Qiu et al., 2020). Moreover, microwave remote sensing data is limited to sampling soil moisture in the first several centimeters of the soil profile, which may not have any correlation with soil moisture content in the root-zone. In this study, 4 cm surface soil moisture was used, and in Song et al. (2022) study, it was found that the deviations between TSEB-SM model performance when using soil moisture data measured at 4 cm, 20 cm, 40 cm, or 80 cm were not significant. This result, is likely due to the soil moisture conditions at this study site and is probably not applicable in other areas. Therefore, it may still be worth considering that in combination with LST used as a proxy of water availability in the root zone, one can better constrain *ET* and the partitioning into plant transpiration and soil evaporation in other regions (Ait Hssaine et al., 2018, 2021). The TSEB-SM modeling scheme described in this study also provides a framework to develop such an approach.

The Sentinel-1 active microwave sensor can deliver 20 m resolution surface soil moisture. The radar backscatter retrieval algorithm derives surface soil moisture at a 20-m ground resolution using a machine learning approach (Greifeneder et al., 2021). Yet, the C-band on Sentinel-1 is significantly more sensitive to vegetation density, limiting its utility for many agricultural crops when they reach maximum biomass. However, the L-band retrievals available from the upcoming NASA-ISRO Synthetic Aperture Radar (NISAR) mission (expected by 2023) should improve upon the (C-band) Sentinel-1 surface soil moisture product with similar spatial resolution (https://nisar.jpl.nasa.gov/). In particular, NISAR's L-band capability should improve the ability to resolve surface soil moisture under dense vegetation cover. In addition, improvements in the temporal responsiveness of LST-based *ET* observations have been achieved by augmenting the Harmonized Landsat and Sentinel-2 surface reflectance (Claverie et al., 2018) dataset with Sentinel-2-sharpened VIIRS (Visible Infrared Imaging Radiometer Suite) as a LST proxy source. This will increase a potential combined frequency of every 2–3 day observation using the TSEB-based approach (Xue et al., 2021). Thus, the potential of combining NISAR surface soil moisture information with more frequent LST sources will allow to TSEB-SM to be evaluated over a full range of land cover and environmental conditions at the field scale.

6. Conclusion

In this study, the performance in heat flux estimation from the TSEB-SM model using both the land surface temperature and near surface soil moisture derived from microwave measurements as key boundary conditions and the original TSEB model which relies on land surface temperature combined with fractional vegetation cover to constrain heat flux estimation are evaluated. Model output of the surface fluxes were assessed using observations from EC flux tower network and four pairs of LAS systems over irrigated agriculture and villages during the HiWATER experiment in 2012. Model performance was similar using both models. The TSEB and TSEB-SM performed similarly over the irrigated agricultural area. However, under the low vegetation cover/dry soil surface moisture conditions in the surrounding arid ecosystem, the TSEB-SM yielded better agreement with observed *H* and *LE* compared to the default soil aerodynamic resistance formulations used in TSEB and appeared to yield better partitioned *LE* from the soil and canopy.

CRediT authorship contribution statement

Yanhao Xu: Writing – original draft, Visualization. **Lisheng Song:** Writing – original draft, Methodology, Supervision. **William P. Kustas:** Review & editing. **Kejia Xue:** Software. **Shaomin Liu:** Resources. **Mingguo Ma:** Resources. **Tongren Xu:** Resources. **Long Zhao:** .

Declaration of Competing Interest

The authors declare that they have no known competing financial interests or personal relationships that could have appeared to influence the work reported in this paper.

Acknowledgement

This work was supported by the National Natural Science Foundation of China (42071298). This research was supported in part by the U.S. Department of Agriculture, Agricultural Research Service. Mention of trade names or commercial products in this publication is solely for the purpose of providing specific information and does not imply recommendation or endorsement by the U.S. Department of Agriculture. USDA is an equal opportunity provider and employer.

References

Agam, N., Anderson, M.C., Kustas, W.P., Norman, J.M., Colaizzi, P.D., Howell, T.A., Prueger, J.H., Meyers, T.P., Wilson, T.B., 2010. Application of the Priestley-Taylor approach in a two-source surface energy balance model. J. Hydrometeorol. 11, 185–198.

Ait Hssaine, B., Merlin, O., Ezzahar, J., Ojha, N., Er-Raki, S., Khabba, S., 2020. An evapotranspiration model self-calibrated from remotely sensed surface soil moisture, land surface temperature and vegetation cover fraction: application to disaggregated SMOS and MODIS data. Hydrol. Earth Syst. Sci. 24, 1781–1803.

Ait Hssaine, B., Chehbouni, A., Er-Raki, S., Khabba, S., Ezzahar, J., Ouaadi, N., Rivalland, V., Merlin, O., 2021. Including radar soil moisture into two-source energy balance model for improving turbulent fluxes estimates. In: 2021 IEEE International Geoscience and Remote Sensing Symposium IGARSS, pp. 6435–6438.

Ait Hssaine, B., Merlin, O., Rafi, Z., Ezzahar, J., Jarlan, L., Khabba, S., Er-Raki, S., 2018. Calibrating an evapotranspiration model using radiometric surface temperature, vegetation cover fraction and near-surface soil moisture data. Agric. For. Meteorol. 256–257, 104–115.

Anderson, M.C., Norman, J.M., Kustas, W.P., Li, F.Q., Prueger, J.H., Mecikalski, J.R., 2005. Effects of vegetation clumping on two-source model estimates of surface energy fluxes from an agricultural landscape during SMACEX. J. Hydrometeorol. 6, 892–909.

Bastiaanssen, W.G.M., Allen, R.G., Droogers, P., D'Urso, G., Steduto, P., 2007. Twenty-five years modeling irrigated and drained soils: State of the art. Agric. Water Manag. 92 (3), 111–125.

Campbell, G.S., Norman, J.M., 1998. An Introduction to Environmental Biophysics.

Chen, J.M., Liu, J., Cihlar, J., Goulden, M.L., 1999. Daily canopy photosynthesis model through temporal and spatial scaling for remote sensing applications. Ecol. Model. 124 (2-3), 99–119.

Cheng, G., Li, X., Liu, S., Xiao, Q., Ma, M., Jin, R., Che, T., Liu, Q., Wang, W., Qi, Y., Wen, J., Li, H., Zhu, G., Guo, J., Ran, Y., Wang, S., Zhu, Z., Zhou, J., Hu, X., Xu, Z., 2013. Heihe watershed allied telemetry experimental research (HiWATER): scientific objectives and experimental design. Bull. Am. Meteorol. Soc. 94, 1145–1160.

Choi, M., Kustas, W.P., Anderson, M.C., Allen, R.G., Li, F., Kjaersgaard, J.H., 2009. An intercomparison of three remote sensing-based surface energy balance algorithms over a corn and soybean production region (Iowa, US) during SMACEX. Agric. For. Meteorol. 149 (12), 2082–2097.

Claverie, M., Ju, J., Masek, J.G., Dungan, J.L., Vermote, E.F., Roger, J.-C., Skakun, S.V., Justice, C., 2018. The Harmonized Landsat and Sentinel-2 surface reflectance data set. Remote Sens. Environ. 219, 145–161.

De Kauwe, M.G., Kala, J., Lin, Y.S., Pitman, A.J., Medlyn, B.E., Duursma, R.A., Abramowitz, G., Wang, Y.P., Miralles, D.G., 2014. A test of an optimal stomatal conductance scheme within the CABLE Land Surface Model. Geosci. Model Dev. Discuss. 7, 6845–6891.

Entekhabi, D., Njoku, E.G., O'Neill, P.E., Kellogg, K.H., Crow, W.T., Edelstein, W.N., Entin, J.K., Goodman, S.D., Jackson, T.J., Johnson, J., Kimball, J., Piepmeier, J.R., Koster, R.D., Martin, N., McDonald, K.C., Moghaddam, M., Moran, S., Reichle, R., Shi, J.C., Spencer, M.W., Thurman, S.W., Tsang, L., Van Zyl, J., 2010. The soil moisture active passive (SMAP) mission. Proc. IEEE 98 (5), 704–716.

Feng, J., Wang, W., Xu, F., Sun, S., 2020. Estimating surface heat and water vapor fluxes by combining two-source energy balance model and back-propagation neural network. Sci. Total Environ. 729, 138724.

Fensholt, R., Langanke, T., Rasmussen, K., Reenberg, A., Prince, S.D., Tucker, C., Scholes, R.J., Le, Q.B., Bondeau, A., Eastman, R., Epstein, H., Gaughan, A.E., Hellden, U., Mbow, C., Olsson, L., Paruelo, J., Schweitzer, C., Seaquist, J., Wessels, K., 2012. Greenness in semi-arid areas across the globe 1981–2007 — an Earth Observing Satellite based analysis of trends and drivers. Remote Sens. Environ. 121, 144–158.

Foken, T., 2008. The energy balance closure problem: an overview. Ecol. Appl. 18 (6), 1351–1367.

Gonzalez-Dugo, M.P., Neale, C.M.U., Mateos, L., Kustas, W.P., Prueger, J.H., Anderson, M.C., Li, F., 2009. A comparison of operational remote sensing-based models for estimating crop evapotranspiration. Agric. For. Meteorol. 149 (11), 1843–1853.

Green, J.K., Seneviratne, S.I., Berg, A.M., Findell, K.L., Hagemann, S., Lawrence, D.M., Gentine, P., 2019. Large influence of soil moisture on long-term terrestrial carbon uptake. Nature 565 (7740), 476–479.

Greifeneder, F., Notarnicola, C., Wagner, W., 2021. A machine learning-based approach for surface soil moisture estimations with google earth engine. Remote Sensing 13 (11), 2099.

Guzinski, R., Nieto, H., Sandholt, I., Karamitilios, G., 2020. Modelling high-resolution actual evapotranspiration through sentinel-2 and sentinel-3 data fusion. Remote Sensing 12 (9), 1433.

Huang, C., Li, Y., Gu, J., Lu, L., Li, X., 2015. Improving estimation of evapotranspiration under water-limited conditions based on SEBS and MODIS data in arid regions. Remote Sensing 7, 16795–16814.

Kowalczyk, E.A., Wang, Y.P., M, L.R., 2006. The CSIRO Atmosphere Biosphere Land Exchange (CABLE) model for use in climate models and as an offline model. Csiro Marine & Atmospheric Research Technical Paper Csiro.

Kustas, W., Anderson, M., 2009. Advances in thermal infrared remote sensing for land surface modeling. Agric. For. Meteorol. 149 (12), 2071–2081.

Kustas, W.P., Zhan, X., Schmugge, T.J., 1998. Combining optical and microwave remote sensing for mapping energy fluxes in a semiarid watershed. Remote Sens. Environ. 64 (2), 116–131.

Kustas, W.P., Jackson, T.J., French, A.N., MacPherson, J.I., 2001. Verification of patch- and regional-scale energy balance estimates derived from microwave and optical remote sensing during SGP97. J. Hydrometeorol. 2 (3), 254–273.

Kustas, W.P., Bindlish, R., French, A.N., Schmugge, T.J., 2003a. Comparison of energy balance modeling schemes using microwave-derived soil moisture and radiometric surface temperature. Water Resour. Res. 39, 1039.

Kustas, W.P., Bindlish, R., French, A.N., Schmugge, T.J., 2003b. Comparison of energy balance modeling schemes using microwave-derived soil moisture and radiometric surface temperature. Water Resour. Res. 39 (2).

Kustas, W.P., Nieto, H., Morillas, L., Anderson, M.C., Alfieri, J.G., Hipps, L.E., Villagarcia, L., Domingo, F., Garcia, M., 2016. Revisiting the paper "Using radiometric surface temperature for surface energy flux estimation in Mediterranean drylands from a two-source perspective". Remote Sens. Environ. 184, 645–653.

Leuning, R., 1995. A critical-appraisal of a combined stomatal-photosynthesis model for C-3 plants. Plant, Cell Environ. 18 (4), 339–355.

Li, X., Cheng, G., Ge, Y., Li, H., Han, F., Hu, X., Tian, W., Tian, Y., Pan, X., Nian, Y., Zhang, Y., Ran, Y., Zheng, Y., Gao, B., Yang, D., Zheng, C., Wang, X., Liu, S., Cai, X., 2018a. Hydrological cycle in the Heihe river basin and its implication for water resource management in endorheic basins. J. Geophys. Res.: Atmospheres 123 (2), 890–914.

Li, F., Kustas, W.P., Anderson, M.C., Jackson, T.J., Bindlish, R., Prueger, J.H., 2006. Comparing the utility of microwave and thermal remote-sensing constraints in two-source energy balance modeling over an agricultural landscape. Remote Sens. Environ. 101 (3), 315–328.

Li, Y., Kustas, W.P., Huang, C., Kool, D., Haghighi, E., 2018b. Evaluation of soil resistance formulations for estimates of sensible heat flux in a desert vineyard. Agric. For. Meteorol. 260–261, 255–261.

Li, Y., Kustas, W.P., Huang, C., Nieto, H., Haghighi, E., Anderson, M.C., Domingo, F., Garcia, M., Scott, R.L., 2019. Evaluating soil resistance formulations in thermal-based two-source energy balance (TSEB) model: implications for heterogeneous semiarid and arid regions. Water Resour. Res. 55 (2), 1059–1078.

Li, D.Z., Jin, R., Zhou, J., Kang, J., 2015. Analysis and reduction of the uncertainties in soil moisture estimation with the L-MEB model using EFAST and ensemble retrieval. IEEE Geosci. Remote Sens. Lett. 12 (6), 1337–1341.

Liu, Y., Kumar, M., Katul, G.G., Feng, X., Konings, A.G., 2020. Plant hydraulics accentuates the effect of atmospheric moisture stress on transpiration. Nat. Clim. Change 10 (7), 691–695.

Liu, S.M., Xu, Z.W., Wang, W.Z., Jia, Z.Z., Zhu, M.J., Bai, J., Wang, J.M., 2011. A comparison of eddy-covariance and large aperture scintillometer measurements with respect to the energy balance closure problem. Hydrol. Earth Syst. Sci. 15, 1291–1306.

Liu, S., Xu, Z., Song, L., Zhao, Q., Ge, Y., Xu, T., Ma, Y., Zhu, Z., Jia, Z., Zhang, F., 2016. Upscaling evapotranspiration measurements from multi-site to the satellite pixel scale over heterogeneous land surfaces. Agric. For. Meteorol. 230, 97–113.

Martens, B., Miralles, D.G., Lievens, H., van der Schalie, R., de Jeu, R.A.M., Fernandez-Prieto, D., Beck, H.E., Dorigo, W.A., Verhoest, N.E.C., 2017. GLEAM v3: satellite-based land evaporation and root-zone soil moisture. Geosci. Model Dev. 10, 1903–1925.

Merlin, O., Dedieu, G., Ceschia, E., Béziat, P., Rivalland, V., Al Bitar, A., 2011. An analytical model of evaporation efficiency for unsaturated soil surfaces with an arbitrary thickness. J. Appl. Meteorol. Climatol. 50, 457–471.

Norman, J.M., Kustas, W.P., Humes, K.S., 1995. Source approach for estimating soil and vegetation energy fluxes in observations of directional radiometric surface temperature. Agric. For. Meteorol. 80.

Oki, T., Kanae, S., 2006. Global hydrological cycles and world water resources. Science 313 (5790), 1068–1072.

Reynolds, J.F., Smith, D.M.S., Lambin, E.F., Turner, B.L., Mortimore, M., Batterbury, S.P. J., Downing, T.E., Dowlatabadi, H., Fernández, R.J., Herrick, J.E., Huber-Sannwald, E., Jiang, H., Leemans, R., Lynam, T., Maestre, F.T., Ayarza, M., Walker, B., 2007. Global desertification: building a science for dryland development. Science 316 (5826), 847–851.

Rigden, A.J., Salvucci, G.D., 2017. Stomatal response to humidity and CO2 implicated in recent decline in US evaporation. Glob. Change Biol. 23, 1140–1151.

Song, L., Kustas, W.P., Liu, S., Colaizzi, P.D., Nieto, H., Xu, Z., Ma, Y., Li, M., Xu, T., Agam, N., Tolk, J.A., Evett, S.R., 2016. Applications of a thermal-based two-source energy balance model using Priestley-Taylor approach for surface temperature partitioning under advective conditions. J. Hydrol. 540, 574–587.

Song, L., Ding, Z., Kustas, W.P., Xu, Y., Zhao, G., Liu, S., Ma, M., Xue, K., Bai, Y., Xu, Z., 2022. Applications of a thermal-based two-source energy balance model coupled to surface soil moisture. Remote Sens. Environ. 271, 112923.

Tanner, C.B., Jury, W.A., 1976. Estimating evaporation and transpiration from a row crop during incomplete cover. Agron. J. 68, 239–241.

Trenberth, K.E., Fasullo, J.T., Kiehl, J., 2009. Earth's global energy budget. Bull. Am. Meteorol. Soc. 90 (3), 311–324.

Twine, T.E., Kustas, W.P., Norman, J.M., Cook, D.R., Houser, P.R., Meyers, T.P., Prueger, J.H., Starks, P.J., Wesely, M.L., 2000. Correcting eddy-covariance flux underestimates over a grassland. Agric. For. Meteorol. 103 (3), 279–300.

Xu, T., Chen, F., He, X., Barlage, M., Zhang, Z., Liu, S., & He, X., 2021. Improve the performance of the noah-MP-crop model by jointly assimilating soil moisture and vegetation phenology data. J. Adv. Modeling Earth Syst. 13, e2020MS002394.

Xue, J., Anderson, M.C., Gao, F., Hain, C., Yang, Y., Knipper, K.R., Kustas, W.P., Yang, Y., 2021. Mapping daily evapotranspiration at field scale using the harmonized landsat and sentinel-2 dataset, with sharpened VIIRS as a sentinel-2 thermal proxy. Remote Sensing 13 (17), 3420.

Zhao, W., Wen, F., Wang, Q., Sanchez, N., Piles, M., 2021. Seamless downscaling of the ESA CCI soil moisture data at the daily scale with MODIS land products. J. Hydrol. 603, 126930.

Zhou, J., Zhang, X., Zhan, W., Gottsche, F.-M., Liu, S., Olesen, F.-S., Hu, W., Dai, F., 2017. A thermal sampling depth correction method for land surface temperature estimation from satellite passive microwave observation over barren land. IEEE Trans. Geosci. Remote Sensing 55 (8), 4743–4756.

Further reading

Ait Hssaine, B., Chehbouni, A., Er-Raki, S., Khabba, S., Ezzahar, J., Ouaadi, N., Ojha, N., Rivalland, V., Merlin, O., 2021. On the utility of high-resolution soil moisture data for better constraining thermal-based energy balance over three semi-arid agricultural areas. Remote Sensing 13 (4), 727.

Bindlish, R., Kustas, W.P., French, A.N., Diak, G.R., Mecikalski, J.R., 2001. Influence of near-surface soil moisture on regional scale heat fluxes: model results using microwave remote sensing data from SGP97. IEEE Trans. Geosci. Remote Sens. 39, 1719–1728.

Fang, L., Zhan, X., Yin, J., Liu, J., Schull, M., Walker, J.P., Wen, J., Cosh, M.H., Lakhankar, T., Collins, C.H., Bosch, D.D., Starks, P.J., 2020. An Intercomparison study of algorithms for downscaling SMAP radiometer soil moisture retrievals. J. Hydrometeorol. 21, 1761–1775.

Guswa, A.J., 2010. Effect of plant uptake strategy on the water−optimal root depth. Water Resour. Res. 46 (9).

Guzinski, R., Anderson, M.C., Kustas, W.P., Nieto, H., Sandholt, I., 2013. Using a thermal-based two source energy balance model with time-differencing to estimate surface energy fluxes with day–night MODIS observations. Hydrol. Earth Syst. Sci. 17, 2809–2825.

Holmes, T.R., Hain, C., Crow, W.T., Anderson, M.C., Kustas, W.P., 2018. Microwave implementation of two-source energy balance approach for estimating evapotranspiration. Hydrol. Earth Syst. Sci. 22, 1351–1369.

Kun, Y., Jiemin, W., 2008. A temperature prediction–correction method for estimating surface soil heat flux from soil temperature and moisture data. Sci. China Ser. D: Earth Sci. 51, 1–9.